International Journal of Biological Macromolecules 318 (2025) 144937

Contents lists available at ScienceDirect

International Journal of Biological Macromolecules

journal homepage: www.elsevier.com/locate/ijbiomac

# Microencapsulation of natural antioxidant-rich and pH-sensitive extracts from Peruvian purple corn (*Zea mays* L.) cob using spray-drying☆

Milagros Sofia Bustamante-Bernedo [a,*], Lizbet León Félix [b], Nils Leander Huamán-Castilla [c], Silvia Ponce [b], David G. Pacheco-Salazar [a]

[a] Laboratorio de Películas Delgadas y Nanomateriales, Escuela Profesional de Física, Universidad Nacional de San Agustín de Arequipa, Av. Independencia s/n, Arequipa, Peru
[b] Grupo de Investigación en Nanomateriales Aplicados, Instituto de Investigación Científica (IDIC), Universidad de Lima, Av. Javier Prado Este, 4600 Surco, Lima 33, Peru
[c] Escuela Profesional de Ingeniería Agroindustrial, Universidad Nacional de Moquegua, Prolongación Calle Ancash s/n, Moquegua 18001, Peru

ARTICLE INFO

*Keywords:*
Purple corn cob
Microencapsulation
Natural antioxidants
Spray-drying
pH-sensitive
Color stability

ABSTRACT

The development of pH-sensitive microcapsules based on natural antioxidants from Peruvian purple corn (*Zea mays* L.) cob was successfully achieved using various wall materials, including maltodextrin, gum arabic, and soy protein isolate, via spray drying. The proportions of wall materials were optimized using a mixed simplex-centroid design, resulting in a microencapsulation efficiency of 95–98 %. The total polyphenol content was 2–3 mg of gallic acid equivalents per g of microcapsules, while the anthocyanin content was 2–3 mg/g of microcapsules. The physicochemical properties of the resulting microencapsulated anthocyanin-rich powders (MAP) were evaluated at different intervals (0 and 48 h) and pH levels (4, 7, and 10). The microcapsules exhibited remarkable color stability ($\Delta E^* < 1$) at pH 4 and 7 over 48 h, with minimal variations in the a* values across pH levels, demonstrating their capacity to retain the characteristic red hue of anthocyanin over time and across varying pH conditions. A structural X-ray diffraction (XRD) analysis showed a semicrystalline structure in all formulations. Fourier-transform infrared (FTIR) analysis revealed that the anthocyanin extract interacted with the wall materials through hydrogen bonding and hydrophobic interactions. The morphological analysis by scanning electron microscopy (SEM) showed that microcapsules with equal proportions of encapsulating agents exhibited fewer surface irregularities than those made with single-wall materials. These results underscore the stability of microcapsules, highlighting their potential as natural antioxidants for applications in the food industry and intelligent packaging.

## 1. Introduction

Purple corn (*Zea mays* L.), a native cereal of Peru, is recognized for its high polyphenol content, present in both the grain and the cob [1]. In particular, the cob contains different families of flavonoids, including anthocyanins, flavonols, and flavones, as well as non-flavonoid compounds such as phenolics and stilbenes. These bioactive compounds can be synthesized through distinct enzymatic pathways [2], contributing to the antioxidant capacity of purple corn and positioning it as a functional ingredient with significant potential health benefits.

Natural extracts derived from purple corn cobs are rich in anthocyanins (Cy-3-glucoside, Pg-3-glucoside, Pn-3-glucoside, Cy-3-malonylglucoside, and Cy-3-dimalonylglucoside) [3] and exhibit promising antioxidant potential by functioning as reducing agents and hydrogen donors [4,5]. These results align with findings from a study conducted in Arequipa, Peru, where HPLC analysis confirmed the presence of the same major anthocyanins in purple corn cobs from that region [6]. Studies have shown that natural extracts are more sensitive to environmental changes due to their complex structures [7] when compared to synthetic dyes, particularly in developments such as intelligent packaging [8,9], as well as applications in the pharmaceutical and food industries [10]. Anthocyanins are highly sensitive to

☆ This article is part of a Special issue entitled: 'Protein-based delivery systems' published in International Journal of Biological Macromolecules.

* Corresponding author.
*E-mail addresses:* mbustamantebe@unsa.edu.pe (M.S. Bustamante-Bernedo), nhuamanc@unam.edu.pe (N.L. Huamán-Castilla), sponce@ulima.edu.pe (S. Ponce), dpachecos@unsa.edu.pe (D.G. Pacheco-Salazar).

https://doi.org/10.1016/j.ijbiomac.2025.144937
Received 16 February 2025; Received in revised form 19 May 2025; Accepted 31 May 2025
Available online 4 June 2025
0141-8130/© 2025 The Authors. Published by Elsevier B.V. This is an open access article under the CC BY license (http://creativecommons.org/licenses/by/4.0/).

environmental factors such as pH, light, oxygen, and high temperatures, which cause their degradation and oxidation [11]. This degradation leads to a loss of color and antioxidant properties, limiting their application in active products. Changes in pH significantly affect their chemical structure. For example, anthocyanins exhibit high stability at a pH of 2–3, while their stability decreases significantly under neutral and alkaline conditions [8,12]. The color variations of anthocyanin-rich solutions in a pH range (2−10) include transitions from the red flavylium cation to the purple/blue quinoidal base, colorless carbinol pseudobase, and yellow chalcone [4,13]. These color changes are significant because color is a key parameter that reflects the preservation of anthocyanins. Given the high sensitivity of anthocyanins, it is crucial to explore advanced technologies to preserve their functional and bioactive properties [14,15]. Among current technologies, spray drying is an efficient process for transforming a liquid medium into powder by atomizing the liquid feed into the hot gas stream. The minimal contact time between the liquid droplets and the drying air enables rapid solvent evaporation, leading to the formation of dry particles. This technique presents several advantages for industrial-scale microencapsulation, including low operational costs, high productivity, and compatibility with a wide range of encapsulating agents [16], making it a highly suitable option for commercial applications. However, when considering scalability, certain limitations must be addressed. The high processing temperatures may compromise the integrity of thermosensitive bioactive compounds, requiring the optimization of operation conditions or the use of protective encapsulating formulations.

In this regard, the inlet and outlet air temperatures (drying temperature) are critical parameters that strongly influence the physical and chemical properties of the resulting powder, including moisture content, particle morphology, and compound stability [17]. Spray drying has proven particularly effective for the encapsulation of thermolabile bioactive compounds, such as anthocyanins, as it preserves their stability and protects them through carrier agents [9,18]. Beyond improving extract stability, the resulting powders also reduced transportation and storage costs, enhancing their industrial value [19]. Moreover, the synergistic use of multiple wall materials has improved encapsulation efficiency and overall powder stability [20–23]. Therefore, the strategic selection of cost-effective, functional, and food-safe biopolymers is crucial to ensuring the scalability and economic viability of the microencapsulation process, particularly for commercial-scale production of bioactive compounds. Among these, proteins stand out as food-grade biopolymers that are generally recognized as safe (GRAS), making them highly suitable for such applications [24]. For example, Khalifa et al. [25] reported that combining whey protein with maltodextrin and gum arabic enhanced the stability of polyphenols, and their antioxidant capacity provided superior functional properties to encapsulated mulberry juice particles. Similarly, Lacerda et al. [26] developed microcapsules of phenolic extracts with excellent physicochemical stability and favorable functional properties using food grade wall materials such as starch, inulin, and maltodextrin as wall materials. However, few studies have been conducted exploring the encapsulation of anthocyanin-rich extracts from purple corn (*Zea mays* L.) cob by spray drying. Thus, the aim of this study is to analyze several formulations of anthocyanin microcapsules, focusing on their antioxidant capacity, pH-dependent color stability over time, and microstructural properties, with potential applications in various fields, including the food industry and active and intelligent packaging systems.

## 2. Material and methods

### 2.1. Material

Raw material, purple corn (*Z. mays* L.) cobs was purchased directly from a local market in Arequipa, Perú. The cobs were dried at 35 °C using a forced-air convection dryer (Memmert, UF55, Germany). Citric acid anhydrous (Scharlau), maltodextrin (MD) with a dextrose equivalent (DE = 10–15), soy protein (SP) with a purity of ≥90 %, and gum arabic (GA) were purchased from Oregon Chem Group (Lima, Perú). All reagents were of analytical grade.

### 2.2. Extraction of anthocyanins-rich extract from purple corn cob

The purple corn cob extracts (PCCE) were obtained using an acidified solution of 60 % (v/v) ethanol in water (1:20 ratio) [27] in an ultrasonic bath (EMAG UC-20 SD, Germany) operating at 45 KHz for 1 h. Finally, the PCCE was stored in amber glass bottles at 10 °C until further use.

### 2.3. Microencapsulation using spray drying

The encapsulation process of anthocyanin-rich extracts by spray drying was designed using a (3,3) simplex-centroid design, involving three wall materials (MD, SP, and GA) in proportions detailed in Table 1, resulting in 10 experiments. Encapsulating agent solutions were prepared at a concentration of 30 % (w/v) by dissolving 30 g of wall materials (MD, SP, and GA) in 100 mL of distilled water, according to the specified proportions. The preparation was initiated with the dispersion of MD in distilled water, followed by magnetic stirring for 1 h. The MD solution was then mixed with SP under continuous stirring for an additional hour, after which GA was added and stirred for another hour. All steps were conducted at 500 rpm and at room temperature. Following this, the matrix solution was kept at rest for 12 h. Subsequently, 100 mL of the PCCE was added to the matrix solutions and stirred at 700 rpm for 3 h to produce a homogeneous suspension.

The resultant solutions were introduced into the primary chamber via a peristaltic pump at room temperature while continuously stirred. The drying process was performed in a mini spray Dryer (Model B-290, Buchi, Switzerland). In all experiments, the inlet temperature was 160 °C, the outlet temperature was 90 ± 5 °C, and a feed rate was 4.8 mL/min, nozzle diameter of 0.7 mm, and an aspiration rate of 75 %. Microencapsulated anthocyanin-rich powders (MAP) obtained were vacuum-sealed and stored in a desiccator at 23 °C and 28 % relative humidity (RH) for further physicochemical analyses.

### 2.4. Characterization

#### 2.4.1. Encapsulation efficiency (%EE)

The encapsulation efficiency was evaluated following the method applied by Zhang et al., [28] with some modifications. Initially, 100 mg of MAP was mixed with 1 mL of distilled water in a vial. This dispersion was vortexed for 1 min and carried out under the ultrasonic bath described above for 30 min. Next, 9 mL of ethanol was added, and the microcapsules were left to act for 5 min before being filtered using Whatman filter paper. The resulting dispersions were then analyzed to calculate the total anthocyanin content (TAC).

To determine the surface anthocyanin content (SAC) of the microcapsules, 100 mg of was mixed with 10 mL of ethanol. The mixture was

**Table 1**
Blends of wall materials obtained by the simplex-centroid design of microcapsulated anthocyanin-rich powders; MD = maltodextrin, SP = soy protein; GA = gum arabic.

| Samples | MD | SP | GA |
|---|---|---|---|
| M1 | 1.000 | 0.000 | 0.000 |
| M2 | 0.000 | 1.000 | 0.000 |
| M3 | 0.000 | 0.000 | 1.000 |
| M4 | 0.500 | 0.500 | 0.000 |
| M5 | 0.500 | 0.000 | 0.500 |
| M6 | 0.000 | 0.500 | 0.500 |
| M7 | 0.333 | 0.333 | 0.334 |
| M8 | 0.670 | 0.165 | 0.165 |
| M9 | 0.165 | 0.670 | 0.165 |
| M10 | 0.165 | 0.165 | 0.670 |

vortexed for 20 s and then centrifuged at 3000 rpm for 5 min at room temperature. The supernatant was collected and filtered. Quantifications were carried out according to the pH differential method described by Giusti & Wrolstad [29]. Two volumes of the extract were diluted in pH 1.0 buffer solutions (0.025 M potassium chloride) and pH 4.5 buffer solutions (sodium acetate) in separate 10 mL volumetric flasks. The dilutions were allowed to equilibrate for 30 min in the dark at room temperature. Following this, each buffer solution was simultaneously measured at 530 nm and 700 nm in a UV–Vis spectrophotometer (Shimadzu UV-1800). The concentration (cyanidin-3-glucoside equivalent, C3G) of anthocyanins was calculated according to the absorbance difference using the following Eq. (1).

$$TAC(mg/L) = \frac{A \times MW \times DF \times 1000}{\varepsilon \times L} \quad (1)$$

where A is equals to $(Abs510nm\text{-}Abs700nm)_{pH\ 1.0} - (Abs510nm\text{-}Abs700nm)_{pH\ 4.5}$, MW is the molecular weight of cyanidin-3-glucoside or C3G (449.2 g/mol); DF is the total dilution factor of sample; ε is the molar extinction coefficient of cyanidin-3-glucoside (26,900 L/($mol^{-1}$.$cm^{-1}$)); L is the path length of cuvette (1 cm). Encapsulation efficiency (%EE) was calculated using Eq. (2), based on the results obtained from TAC and the surface anthocyanin content (SAC).

$$EE(\%) = \frac{TAC - SAC}{TAC} \times 100\% \quad (2)$$

### 2.4.2. Total phenolic content (TPC)

The total polyphenol content (TPC) and antioxidant capacity of MAP were calculated using the method detailed by Parí et al. [30] with modifications. A preliminary treatment was utilized to extract anthocyanins from MAP. For TPC, 0.5 g of sample powder was dissolved in 50 mL of distilled water, stirred for 2 min, and stored in the dark for approximately 1 h. Subsequently, the supernatant was passed through a 0.2 μm pore nylon syringe filter and collected in a falcon tube for further analysis. The samples were evaluated using a Microplate Reader (Synergy/HTX, Biotek Instruments Inc., Winooski, VT, USA), and the absorbance was measured at 765 nm. TPC was expressed as mg of gallic acid equivalents (GAE) per g of microcapsules (mg GAE/g of microcapsules), utilizing a standard curve of gallic acid (20 mg/mL–80 mg/mL).

### 2.4.3. Moisture and drying yield

The percentage of moisture content in the microcapsules was determined using a humidity balance (OHAUS, MB120, País). Additionally, the % of drying yield was evaluated using Eq. (3) [31].

$$Drying\ yield\ (\%) = \frac{powder\ after\ spray\ drying(g)}{solids\ in\ feed\ solution(g)} \times 100\% \quad (3)$$

### 2.4.4. Color measurement

The color of microcapsules was measured by using an Avaspec-ULS2048XL detector (Avantes). Initially, the powders were put in a photo box with a light bulb source, and images were captured from the top of the samples by a high-resolution mobile camera. Colorimetric analysis was performed with a 50 mm integrating sphere (AvaSphere-50-LS-HAL-12V) equipped with a calibration lamp (NIST standard accuracy) to measure the color parameters ($L^*$, $a^*$, and $b^*$). The total color difference (ΔE*) was calculated using the following Eq. (4).

$$\Delta E^* = \sqrt{\left(L_o^* - L^*\right)^2 + \left(a_o^* - a^*\right)^2 + \left(b_o^* - b^*\right)^2} \quad (4)$$

where L*, a*, and b* are values that represent brightness, intensity of red and green and intensity of yellow and blue of the color parameters of the powders, respectively, and $L_o^*$ (96.21), $a_o^*$ (1.28), and $b_o^*$ (25.77) represent the standard parameters of the plate used as the background.

A color difference of 0 to 1.5 can be considered small and imperceptible to visual observation; in the 1.5 to 5 intervals, the color difference can be distinguished, while the total color difference can be evident for ΔE higher than 5.

### 2.4.5. Color variations response to different buffer solutions at pH 4–7-10 (0 and 48 h) of the MAP

A 20 mg sample of microcapsules was dissolved in 10 mL of buffer solutions at pH 4, 7, and 10, followed by stirring for 1 h Color changes of each solution were recorded at intervals of 0, and 48 h.

### 2.4.6. X-ray diffraction (XRD)

XRD patterns of the PCCE, wall materials, and spray-dried powders were measured using a Siemens (Rigaku) diffractometer operating at 40 kV and 15 mA with Cu K$\alpha$ radiation ($\alpha = 1.5418$ Å). Diffractograms were taken between 5° and 60° at a scan speed of 2°/min and with a step size of 0.02.

### 2.4.7. Scanning electron microscopy (SEM)

Particle structures of the microcapsules were evaluated by a Thermo Scientific Scios 2 Dual Beam microscope. The microcapsules were deposited on a-sided carbon conductive tape and coated with a thin layer of gold. An accelerating voltage of 15 kV was used during the experiments. The SEM images of MAP were analyzed using ImageJ software to determine the mean diameter.

### 2.4.8. Fourier-transform infrared (FTIR)

The identification of functional groups on the surfaces of microcapsules and the interactions between PCCE and the wall materials were conducted using a Fourier-transform infrared (FTIR) spectrophotometer (Shimadzu IRTracer-100 Model) under an attenuated total reflectance (ATR) mode. The analysis was performed with a resolution of 2 $cm^{-1}$ in the wavenumber range of 4000–400 $cm^{-1}$ with 32 scans.

### 2.5. Statistical analysis

All numerical results in this study are presented as the mean value ± standard deviation based on triplicates performed for each characterization test, except for the product yield, which was determined from a single spray-drying process that produced a significant amount of powder/microparticles in one batch. Statistical differences among treatments were evaluated using one-way analysis of variance (ANOVA) followed by Tukey's post hoc test, performed with Minitab software (version 18.0) at a 95 % confidence level ($P < 0.05$).

## 3. Results and discussion

### 3.1. Characterization of MAP

The results of moisture content, drying yield (%), encapsulation efficiency (%EE), total phenolic content (TPC), and anthocyanin content of the microcapsules produced using various combinations of wall materials are summarized in Table 2.

The moisture content for all combinations of microcapsules was <10 %, varying from 3.34 % to 5.60 %. Formulations containing only MD, SP, and GA (M1, M2, and M3, respectively) exhibited low moisture content (<4 %). M6 showed the highest moisture content (~6 %) among all formulations. Variations in moisture content among samples depend on carrier agent types and concentrations. Moisture plays a critical role in determining the glass transition and crystallization behavior of the powders [32,33]. These moisture values favor the stability of the capsules during storage [15] and are consistent with values previously reported for spray-dried powders. Furthermore, moisture content is a key parameter influencing drying efficiency, flowability, viscosity, and overall storage stability, as it directly affects the glass transition temperature and crystallization dynamics. Regarding stability, the encapsulation efficiency (%EE) of all microcapsules exceeded 95 %, indicating

**Table 2**
Moisture content (%), drying yield (%), %EE, anthocyanins, and TPC of the powders.

| T | MD | SP | GA | Moisture (%) | Drying yield (%) | %EE | Anthocyanins MAP (mg/g) | TPC (mg/g of microcapsules) |
|---|---|---|---|---|---|---|---|---|
| M1 | 1.000 | 0.000 | 0.000 | $3.83 \pm 0.09^{cd}$ | 79.43 | $96.40 \pm 0.05^{cd}$ | $2.88 \pm 0.04^{f}$ | $3.4 \pm 0.1^{b}$ |
| M2 | 0.000 | 1.000 | 0.000 | $3.45 \pm 0.10^{d}$ | 45.87 | $95.30 \pm 0.04^{d}$ | $3.35 \pm 0.03^{c}$ | $2.88 \pm 0.06^{def}$ |
| M3 | 0.000 | 0.000 | 1.000 | $3.34 \pm 0.40^{d}$ | 80.30 | $98.2 \pm 0.5^{ab}$ | $3.77 \pm 0.02^{a}$ | $3.9 \pm 0.2^{a}$ |
| M4 | 0.500 | 0.500 | 0.000 | $5.0 \pm 0.5^{ab}$ | 40.97 | $97.8 \pm 0.3^{abc}$ | $3.35 \pm 0.01^{c}$ | $2.8 \pm 0.1^{ef}$ |
| M5 | 0.500 | 0.000 | 0.500 | $3.6 \pm 0.7^{d}$ | 75.87 | $97.9 \pm 0.7^{abc}$ | $2.74 \pm 0.02^{g}$ | $3.90 \pm 0.09^{a}$ |
| M6 | 0.000 | 0.500 | 0.500 | $5.6 \pm 0.2^{a}$ | 57.83 | $98.5 \pm 0.8^{a}$ | $2.24 \pm 0.01^{h}$ | $2.58 \pm 0.07^{f}$ |
| M7 | 0.333 | 0.333 | 0.334 | $4.2 \pm 0.5^{abc}$ | 60.27 | $98.1 \pm 0.9^{ab}$ | $3.55 \pm 0.03^{b}$ | $3.2 \pm 0.2^{bcd}$ |
| M8 | 0.670 | 0.165 | 0.165 | $3.6 \pm 0.3^{d}$ | 68.80 | $97.1 \pm 0.5^{abc}$ | $3.75 \pm 0.03^{a}$ | $2.89 \pm 0.08^{def}$ |
| M9 | 0.165 | 0.670 | 0.165 | $4.1 \pm 0.1^{bcd}$ | 43.23 | $98.1 \pm 0.3^{ab}$ | $3.02 \pm 0.03^{e}$ | $2.95 \pm 0.01^{cde}$ |
| M10 | 0.165 | 0.165 | 0.670 | $4.8 \pm 0.4^{abc}$ | 66.23 | $96.8 \pm 0.6^{bcd}$ | $3.25 \pm 0.01^{d}$ | $3.3 \pm 0.2^{bc}$ |

Means in each column with different superscript letters are significantly different ($p < 0.05$).

effective retention of active compounds. The highest %EE values were observed in formulations M3 (98.2 %), M6 (98.5 %), M7 (98.1 %), and M9 (98.1 %), indicating excellent encapsulation performance. In contrast, formulation M2, which used only SP as the encapsulating agent, showed the lowest efficiency (95.3 %). The use of GA can significantly enhance encapsulation efficiency; for instance, in formulation M3, GA alone achieved the highest %EE, likely due to its ability to form a protective layer around the core material, reducing exposure to air. MD also showed high encapsulation efficiency and drying yield in formulation M1, which may be attributed to its ability to form an amorphous glass structure [34]. Conversely, the lower performance of SP alone in M2 suggests limited encapsulation capacity without synergistic interactions with other wall materials. This protective effect minimizes the susceptibility of the flavylium cation in anthocyanins to nucleophilic attack by water molecules, thus enhancing their structural stability and prolonging their bioactive properties [35]. As a result, the high %EE is attributed to the superior retention capacity of the wall materials, which effectively trap the core material and minimize its surface deposition on the microcapsules. These findings emphasize the importance of selecting an appropriate carrier composition to optimize encapsulation efficiency across all formulations, ensuring the stability and functionality of the encapsulated active material.

Norkaew et al. [36] reported similar results as those obtained in this study, demonstrating that anthocyanin microparticles prepared with MD, GA, and whey protein isolate achieved encapsulation efficiencies close to 100 %. However, formulation using only whey protein isolate achieved lower efficiency (83 %), which highlights the benefits of combining multiple carrier agents.

The drying yield of the microencapsulated samples was highest in the formulations with a higher content of GA, reaching up to 80.3 %. In contrast, the lowest yield was observed in formulation M4, which used a combination of MD and SP without the addition of GA. This may be attributed to the absence of GA, a carrier agent renowned for its excellent film-forming and emulsion-stabilizing properties. The lack of GA likely reduces process efficiency, leading to increased material loss and lower core protection during the drying process [37].

The TAC of the PCCE was $24.4 \pm 0.5$ mg/g dry weight, expressed as cyanidin-3-glucoside (C3G), the major anthocyanin in purple corn cob. After microencapsulation, the TAC in the MAP, determined by the pH differential method, ranged from 2.24 mg/g (M6) to 3.77 mg/g (M3). The highest anthocyanin retention was observed in the formulation utilizing a GA-based matrix, highlighting its effectiveness as a carrier in the microencapsulation process [38]. Similarly, TPC ranged from 2.58 (M6) to 3.90 (M5) mg/g. Microcapsules M3 and M5 showed the highest TPC values, while M6 showed the lowest, consistent with the anthocyanin content. This finding suggests that the combination of these matrices was optimal for preserving bioactive components.

### 3.2. Color measurement of MAP

The initial color of the powders obtained from the different MAP formulations is shown in Fig. 1. Color values of all formulations were evaluated using the CIELAB parameters such as L*, a*, b*, and ΔE, providing critical insights into the color stability as shown in Fig. 2.

The L* values ranged from 54.32 (M5) to 63.08 (M6), indicating significant variability in lightness among the samples. All formulations exhibited high a* values, ranging from 51.92 (M2) to 56.51 (M10), indicating a strong red coloration. The b* values ranged from −8.34 (M2) to −3.19 (M1), with M2 showing the most negative value, indicative of a blue tone. Moreover, the elevated ΔE value (>3) indicates noticeable color differences among the microcapsules that can be readily distinguished by the human eye.

In the context of active packaging applications using microencapsulation, both samples M6 and M10 demonstrated particularly favorable color characteristics. Sample M6 is notable for its highest luminosity (L* value of 63.08), which enhances visual appeal, a key factor influencing consumer perceptions of freshness and quality of the product. Previous studies have attributed higher L* values to a greater ratio to wall materials relative to the core.

Among all formulations, sample M10 exhibited the highest a* value (56.51), indicating a strong red hue likely associated with higher anthocyanin content and improved encapsulation efficiency. To contextualize this result, Table 3 compares the a* values of M10 with those reported for anthocyanin-based microcapsules in the literature. The emphasis on the a* parameter is justified by its direct correlation with anthocyanin color intensity. M10 showed comparable or superior redness, supporting its potential for active packaging applications where visual impact and bioactivity are essential.

### 3.3. Evaluation of chromatic stability in MAP formulations under different pH conditions and exposure times

This study evaluated the chromatic stability of 10 distinct MAP formulations under varying pH conditions (4, 7, and 10) and two time points (0 and 48 h). The CIELAB parameters were monitored to assess the extent of color change and stability over time. ΔE* values served as the primary indicator of chromatic stability, with lower ΔE* values signifying greater stability. The representative color profiles of all formulations are shown in Fig. 3. Anthocyanins were identified as the key metabolites influencing the a* value [45]. A decline in the a* value over time indicates a reduction in red intensity, likely due to anthocyanin degradation or a shift toward less vibrant hues. This change is particularly critical at pH levels above 7, where anthocyanins are more prone to destabilization, resulting in a diminished red hue. Conversely, when the a* value remains stable or increases, it reflects good retention of red intensity, which is essential for product stability [46].

At pH 4, M8 and M3 demonstrated the highest stability in a* values over the 0 to 48 h period, showing minimal variation. Specifically, M8 exhibited a negligible decrease of only 0.03 (from 9.91 at 0 to 9.88 at 48 h), while M3 decreased by just 0.04 (from 10.41 to 10.37). These results position M8 and M3 as the most stable color-stable formulations under acidic conditions (pH 4), making them preferable for applications when

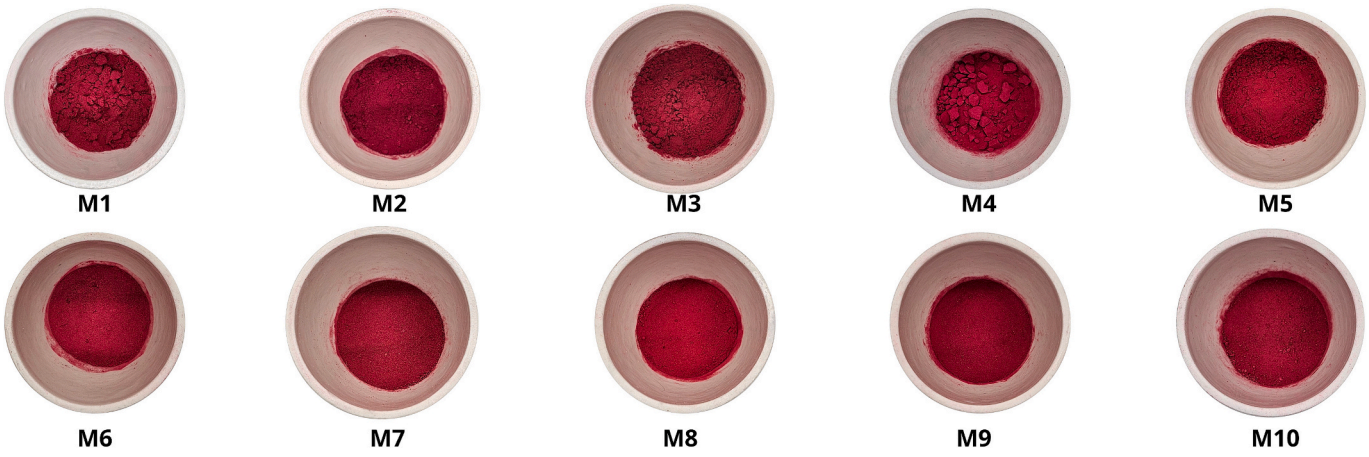



**Fig. 1.** Photos of the different MAP formulations (M1–M10).
MAP: microencapsulated anthocyanin powder.

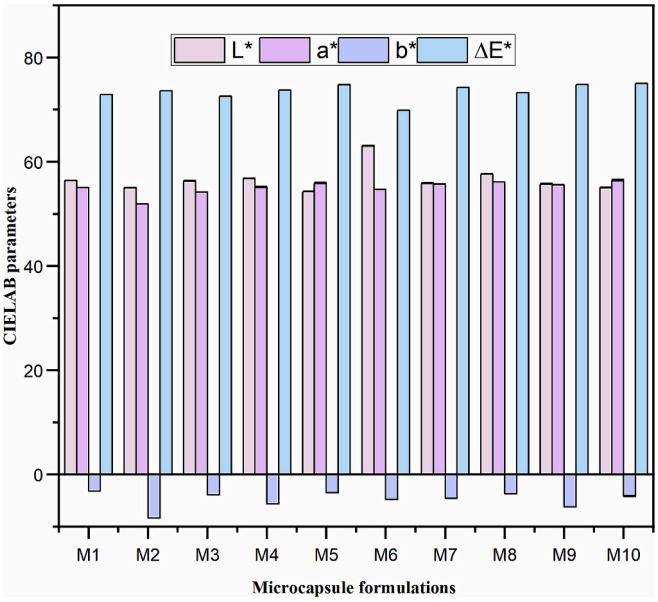



**Fig. 2.** CIELAB color parameters (L*, a*, b*) and total color difference (ΔE*) of the different MAP formulations (M1–M10). L*: lightness; a*: red-green coordinate; b*: yellow-blue coordinate; ΔE*: total color difference.

**Table 3**
Comparative analysis of the a* color parameter in microcapsules containing anthocyanins.

| Anthocyanin source | Wall material | a* | Reference |
|---|---|---|---|
| Purple corn cob | Maltodextrin/soy protein/ gum arabic | 56.51 | This study (M10) |
| Purple corn | Maltodextrin | 30.15 | [39] |
| | Maltodextrin/gum arabic | 28.09 | |
| | Maltodextrin/whey protein isolate | 25.74 | |
| Purple corn pericarp | Maltodextrin | 19.20 | [40] |
| | Gum arabic | 19.05 | |
| | Skim milk powder | 17.31 | |
| Purple corn | Alginate | 42.92 | [41] |
| Wine grape pomace | Gum Arabic/maltodextrin | 16.39 | [42] |
| Blend of jabuticaba, jussara and blueberry | Maltodextrin/whey protein/gum arabic | 25.56 | [43] |
| Red cabbage pomace | Maltodextrin/gum arabic | 27.59 | [44] |

consistent red coloration is essential.

The slight decrease in redness color during storage can be attributed to the degradation of monomeric anthocyanins, as previously reported [47]. While stability in a* values is desirable, an increase is often even more favorable, as it indicates color preservation, and the potential enhancement of the red hue associated with anthocyanins in acidic environments. This interpretation has been linked to the formation of anthocyanin-derived pigments, which contributes to the stabilization of the flavylium cation and reinforces red color retention [48,49].

In this study, M6 exhibited a notable increase in a* values, from 6.95 at 0 to 8.24 at 48 h, representing a total change of 1.29. These results suggest that M6 not only preserves but also enhances color properties over time, supporting its visual quality and potential bioactivity for applications requiring long-term stability. At pH 7, M6 also exhibited the highest stability in a* values from 0 to 48 h, with a difference of 0.96. This minimal change reflects strong color stability, indicating effective preservation of the red hue over time. In contrast, formulation M9 showed the most significant decline in chromatic stability, with an absolute difference of 2.23 in a* value, indicating comparatively lower performance under neutral pH.

At pH 10, M1 exhibited the highest stability in a* values, demonstrating the smallest absolute change of 0.92 (from 5.33 at time 0 to 4.41 at 48 h). In contrast, formulation M7 showed the largest absolute change, with a difference of 4.35. These results highlight M1 as the most stable option under alkaline conditions (pH 10). In the context of anthocyanin stability, the largest changes in a* values in different pH levels (pH 4, 7, and 10) can be interpreted in two ways. While the largest differences may suggest lower stability in the traditional sense, indicating a reduced ability to maintain a consistent red hue, such differences also highlight the inherent pH sensitivity of anthocyanins. Significant color changes at varying pH levels highlight their ability to adapt their hue in response to environmental conditions. This property is particularly advantageous in food and beverage applications, where visual appeal is crucial. Therefore, a formulation exhibiting pronounced color shifts in pH levels should not necessarily be considered unstable; instead, it demonstrates a desirable characteristic of anthocyanins, making them suitable for dynamic formulations where color serves as a quality or freshness indicator.

The L* value reflects color lightness, where an increase in L* suggests a shift to a lighter color, often indicating color fading in anthocyanins under alkaline or neutral conditions. Conversely, a decrease or stable L* value indicates better maintenance of a darker, more saturated color, which enhances visual appeal and supports the perceived potency in anthocyanin-based products. Formulation M5 showed the lowest color variation at pH 4 over 48 h, with an L* change of 0.30. This minimal change indicates excellent color stability and robust color integrity

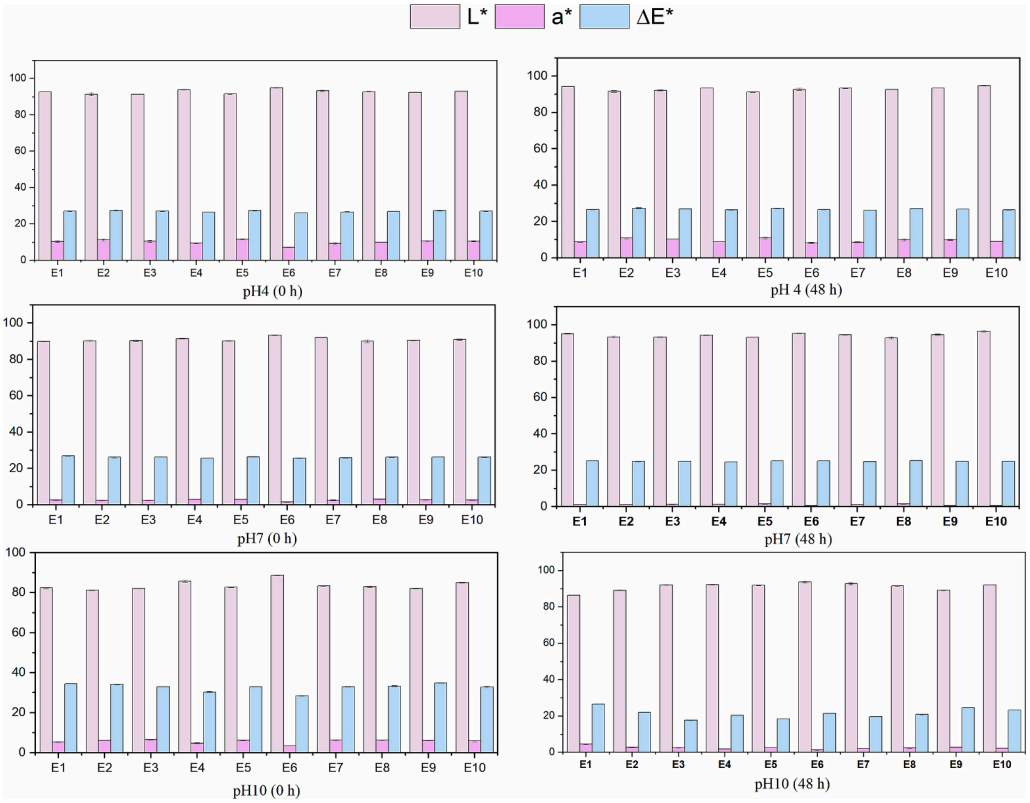



**Fig. 3.** Evaluation of chromatic stability in MAP formulations (M1–M10) exposed at pH 4, 7, and 10 over time (0 and 48 h).

compared to the other formulations tested. On the other hand, M1 demonstrated the greatest change with an increase of 1.67, highlighting its comparatively lowest chromatic stability under acidic conditions.

At pH 7, the L* values of the anthocyanin microcapsules generally increased after 48 h of storage, indicating a shift toward a lighter coloration and suggesting a reduction in color intensity over time. This behavior is consistent with previously reported studies, where an increase in L* during storage has been associated with color fading resulting from anthocyanin degradation [42]. For optimal stability, it is preferable to maintain or minimize changes in L* values over time, as this correlates with greater color retention. Notably, M6 exhibited the smallest increase in L*, with an increase of only 1.96 units at 48 h. These findings underscore the importance of minimizing increases in L* to preserve the functional quality of anthocyanin-based products at pH 7. At pH 10, the L* values of the anthocyanin microcapsules increased after 48 h, indicating a shift toward a lighter color and a decrease in color intensity over time. This rise in L* suggests a potential reduction in the color stability of anthocyanins under alkaline conditions. To ensure optimal stability and preservation of the microcapsule's antioxidant properties, it is preferable for L* values to remain stable or decrease, as the lowest L* values are associated with greater color retention. Hay et al. [45] attributed the decrease in lightness L* and increase in redness a* to the high anthocyanidin content. Notably, the M1 sample exhibited the smallest increase in L*, with a rise of only 4.09 units after 48 h.

The ΔE* value represents the overall color difference between two points in time. An increase in ΔE* suggests a notable color change, indicating a perceptible shift in visual appearance. For anthocyanins, rising ΔE* values indicate alterations in the color matrix due to pH effects or stability factors, which could result in undesired hues. However, if ΔE* remains low, color perception remains stable, ideal for maintaining a consistent red appearance in anthocyanin-based products. The analysis of ΔE* values for the ten formulations at different pH levels (4, 7, and 10) and over time (0 and 48 h) provides valuable insights into their chromatic stability. At time 0, the ΔE* values for all formulations indicate significant color differences compared to the white reference standard. This initial ΔE* variability reflects the inherent differences in the color of the formulations, with some showing higher initial ΔE* values, indicating greater deviations from the reference white. The changes in ΔE* over time and in pH levels allow us to assess the relative stability of each formulation under the experimental conditions. At pH 4, M5 exhibited the highest stability, maintaining a consistent color with no detectable change (ΔE* absolute difference of 0.00). Additionally, M3 showed minimal variation, with differences of 0.02, reflecting relatively stable performance under acid conditions, while M6 showed a notable increase in ΔE* values, with an absolute change of 0.69 (from an initial value of 25.91 at time 0 to 26.6 at 48 h). This notable increase indicates a significant alteration in color, highlighting the formulation's sensitivity to changes in pH and its relatively lower chromatic stability in acidic environments. At pH 7, M6 demonstrated color stability over a 48 h period, with an absolute ΔE* variation of only 0.47 from the initial measurement to 48 h. This result underscores its robustness in maintaining color integrity at this pH level and identifies it as the most stable formulation under neutral conditions. The remarkably low ΔE* values in a neutral pH indicate that M6 is particularly well-suited for applications requiring long-term color consistency, making it an ideal choice for products where visual stability is a critical quality parameter. The microcapsules demonstrated excellent color stability over 48 h at pH 4 and 7, with ΔE* values below 1, signifying imperceptible color changes. This stability highlights their potential for applications in functional packaging and bioactive systems requiring long-lasting color retention. At pH 10, formulation M6 displayed the smallest color variation over 48 h, with an absolute ΔE* change of 6.92 from the initial measurement to 48 h. These results suggest that, in an alkaline environment, M6 maintained color stability more effectively than other formulations.

In conclusion, the stability of MAP at varying pH levels was effectively evaluated by comparing the L*, a*, and ΔE* values at 48 h with their corresponding initial values at time 0. Minimal changes in these parameters suggest that the characteristic color associated with each pH

(4–7–10) remained stable, indicating resistance to color degradation over time. Specifically, stable a* values reflect preserved red intensity, while consistent L* values suggest limited color fading. Additionally, low ΔE* values between 0 and 48 h confirm minimal perceptible color change, supporting the color stability of these microcapsule formulations in different pH environments.

The colorimetric parameters (a*, L*, and ΔE*) calculated for the formulations (M1 to M10) correspond to the observed color changes, as illustrated in the representative image in Fig. 4. Comprehensive visual data for all formulations can be found in the Supplementary material (Fig. S1). Variations in color intensity, especially under different pH conditions (4, 7, and 10) and over time (0 and 48 h), are reflected in the calculated ΔE* values, underscoring the influence of experimental conditions on color stability.

While long-term stability was not assessed in this study, microencapsulation is known to enhance anthocyanin protection and may extend it beyond 48 h. The evaluation period was chosen based on studies using anthocyanin-based films for spoilage monitoring, which indicated significant seafood spoilage between 36 and 48 h, with an average onset occurring around 42 h. [50–53]. During this window, seafood experiences change due to the accumulation of volatile nitrogenous compounds, such as biogenic amines and trimethylamine ammonia. Furthermore, anthocyanin-loaded microcapsules embedded in carrageenan/carboxymethyl cellulose films facilitated real-time monitoring of beef freshness through progressive color changes and reacted to ammonia exposure with distinct visual transitions [54]. It is important to note that the observed color changes result from the inherent pH sensitivity of anthocyanins; even when these pigments are encapsulated, their visual response remains the primary indicator of pH alterations. Previous research has shown that anthocyanin-based pH-sensitive films can effectively detect changes through visible color variations. Therefore, our study design reflects real-world conditions, demonstrating that anthocyanin microcapsules embedded in a polymeric matrix can serve as reliable freshness indicators. Future studies should assess long-term performance under extended storage conditions to explore broader implications and applications. Beyond colorimetric responses, microparticles have also demonstrated additional functional benefits in food systems. Previous studies have shown the applicability of microcapsules in various food systems. For instance, edible films with microcapsules reduced strawberry weight loss by 49.03 % after 10 days. Chitosan-based deep eutectic films enriched with 2 % açaí microparticles exhibited favorable mechanical properties and antioxidant activity, supporting their potential use in active packaging [55]. Similarly, chitosan films that incorporated encapsulated anthocyanins achieved 56 % radical scavenging activity and functioned as barriers against UV and visible light, contributing to the shelf-life extension of blueberries [27]. Collectively, these applications underscore the multifunctionality of microcapsules in smart packaging.

### 3.4. Structural characterization

Fig. 5 shows the X-ray diffraction patterns of the MAP formulations and the structure of the dry PCCE and wall materials are provided in




**Fig. 4.** Visual changes in M7 formulation exposed to different pH (4, 7, 10) over time (0 and 48 h).

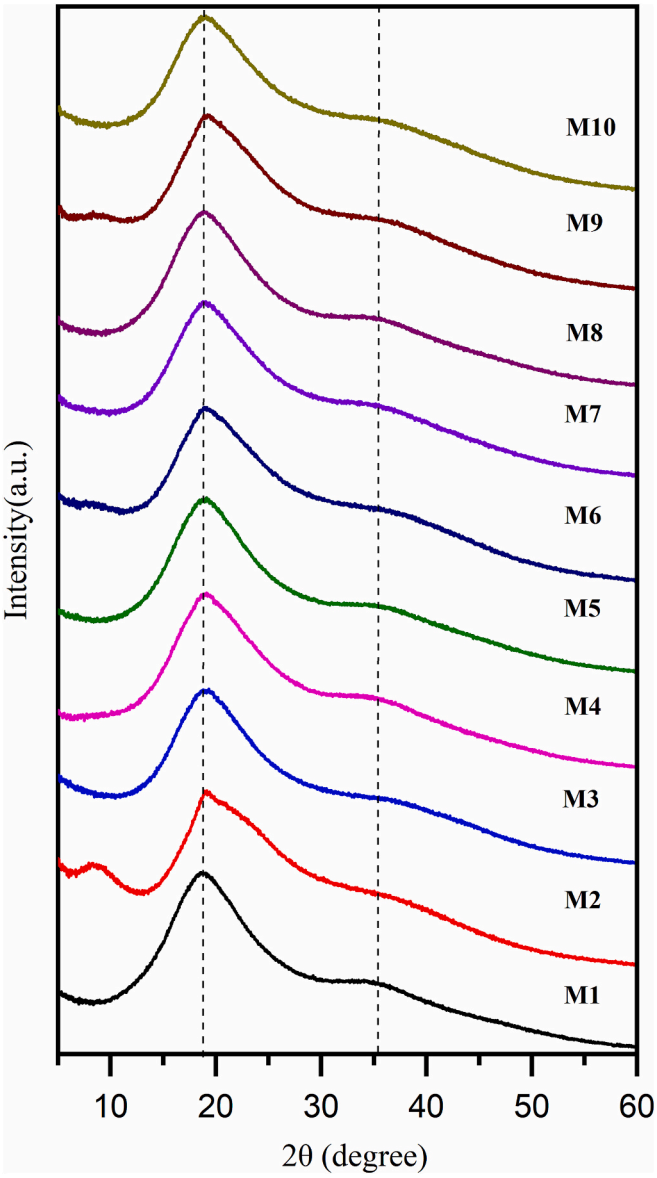



**Fig. 5.** X-ray diffraction (XRD) patterns of MAP formulations (M1–M10).

Fig. S2 of the Supplementary material. The XRD pattern of PCCE evidenced an amorphous structure characterized by a broad diffraction peak around 24°, consistent with the structure of purple corn cob anthocyanins reported by Dai et al. [56]. On the other hand, the wall materials exhibited a semi-crystalline structure. Specifically, MD presents diffraction peaks at around 18.5° and 34.5°, GA displayed diffraction peaks around 18.7°, and SP exhibited diffraction peaks at approximately 8.7°, along with a broad peak around 19° (data is shown in the Supplementary material). Furthermore, samples M1, M2, and M3 evidenced the same diffraction peaks as their respective wall materials (MD, SP, and GA). This evidence showed that the encapsulation process did not alter the structural properties of the wall material. [57]. The X-ray diffractogram of the MAP formulations showed no characteristic diffraction peaks of PCCE, suggesting that it was fully encapsulated within the microcapsules rather than forming a simple physical mixture [58]. This finding aligns with the high encapsulation efficiency (>95 %) observed in all formulations. Additionally, the MAP formulations exhibited a semi-crystalline structure characterized by a broad main peak around 19° and a pronounced shoulder around 35°, regardless of the percentage of wall material in the formulation. The recrystallization of the wall materials appears to modify the structure of PCCE, as

evidenced by the disappearance of its characteristic peak, suggesting strong interactions between PCCE and the wall materials. This recrystallization is likely due to the rapid evaporation during the spray drying process used to produce the microcapsule powder [59]. The results suggest that while the different wall materials did not significantly alter the semi-crystalline properties of the microcapsules, they influenced the crystallinity of PCCE, playing a key role in shaping the final structure of the encapsulated products. Moreover, the higher crystallinity observed in certain formulations implies greater structural stability, consistent with previous studies indicating that crystalline materials are generally more stable than non-crystalline structures [58,60].

The structural properties of these materials play an important role in determining their applications. Amorphous materials exhibit higher solubility compared to crystalline materials due to their structural disorder, which facilitates a rapid dissolution, an important parameter in the beverage industry [61,62]. However, amorphous samples are highly hygroscopic, making them susceptible to moisture absorption during storage. This absorption can lead to stickiness and the formation of agglomerates as amorphous sugars transition into a crystalline state. Such behavior adversely affects storage by causing weight gain, nutrient degradation, microstructural collapse, and increased risk of microbiological instability [63].

Although the XRD diffractograms did not show significant changes in the semi-crystalline structure of the encapsulating matrices, FTIR analysis revealed clear interactions between the encapsulated extract and the wall materials. This observation is consistent with the hypothesis that functionalization can induce surface-level chemical interactions without substantially altering the crystalline lattice. In some cases, the presence of broad humps at low angles is likely due to the formation of amorphous surface layers rather than the development of new well-defined crystalline planes [64]. In this context, FTIR serves as a more sensitive technique for detecting local bonding changes and the presence of specific functional groups.

### 3.5. Morphology

The morphology of all prepared microcapsules was analyzed using SEM images, as shown in Figs. 6–7. It is important to know as it is directly related to manufacturing efficiency, product quality, and instability. Microcapsules prepared with single-wall material (M1, M2, or M3) exhibited non-uniform agglomeration particles, surface indentations, and high polydispersity in particle sizes, being most evident in the sample M2. This sample showed a greater prevalence of surface irregularities and significant particle deformation, which could explain its lower %EE. The irregular and wrinkled surface morphology of microcapsules in all samples is attributed to the rapid evaporation of water during the spray-drying process [36,60]. This process led to the shrinkage of the microcapsules while effectively preserving the phenolic compounds encapsulated within the coacervated structures [65].

Samples M5 and M6 exhibited spherical shapes with high polydispersity in particle sizes. Nevertheless, samples M8, M9, and M10 showed some hollow particles containing small particles inside, likely formed due to expansion during the spray drying process [35]. This could increase gas permeability and compromise the protection and stability of the active material [66]. Also, it was observed that using encapsulating agents in equal proportions, as in sample M7, microcapsules with less irregular surfaces compared to formulations using MD, SP, and GA individually were shown [66]. The shape of the microcapsule is strongly influenced by the physical properties of the encapsulated material. For instance, when the core material is solid or crystalline, the resulting capsules could exhibit irregular shapes. In contrast, when the core material is liquid, the process often yields a spherical capsule containing a single droplet of the active ingredient [67]. Moreover, all formulations exhibited the formation of small particle agglomerates surrounding larger particles, consistent with findings reported in the literature [68]. Maintaining uniform microcapsule size has been shown to be important for applications in the food and pharmaceutical industries. Microcapsules that are too small can reduce the efficiency of core material encapsulation, while overly large particles may lead to undesired aggregation, negatively impacting both the solubility and sensory properties of the encapsulated substances [69]. In general, the surfaces of most formulations were spherical, demonstrating their effectiveness as encapsulating materials. Encapsulation efficiencies exceeding 95 % further highlight their ability to effectively retain the target compounds. Moreover, combining wall materials is widely recognized as an effective strategy for the microencapsulation of bioactive compounds, significantly enhancing their stability. Statistical analysis of the microcapsules size, using log-normal functions to fit the particle size distribution as shown in the inset at the top-left of Figs. 6–7, revealed a mean size ranging from a diameter of 4.8 μm to 10.9 μm, with high polydispersity observed in all samples.

### 3.6. ATR-FTIR

ATR-FTIR was conducted to investigate the interactions between PCCE and polysaccharides to identify any structural changes in the microcapsules resulting from the encapsulation of anthocyanins with wall materials (Fig. 8). It can be seen that PCCE before encapsulation showed characteristic wavelengths at 3314 $cm^{-1}$ because of the stretching vibration of hydroxyl groups O—H bonds that are present in the phenolic groups of the flavonoid molecule and water [70]. The strong band at 1643 $cm^{-1}$ is correlated to the stretching vibration of aromatic C═C groups of purple corn anthocyanins [71], while the band at 1452 $cm^{-1}$ indicates a C═C bond deformation vibration of phenolic groups [72] or a skeleton vibration of the heterocyclic benzopyran ring in the anthocyanins [73] (data are shown in Fig. S3 of the Supplementary material). The spectrum of all microcapsules exhibited a decrease in intensity and a shift to a higher frequency in the hydroxyl group (O—H bonds) stretching region (from 3309 $cm^{-1}$ to 3335–3280 $cm^{-1}$), which could be attributed to the formation of hydrogen bonds between flavonoids and wall materials [74], water removal during the spray-drying process, or the presence of carboxylic acids [21] from the wall materials (SP and GA). The small bands at 2980 and 2903 $cm^{-1}$ are related to the C—H bond stretching of the flavonoid aromatic phenyl ring [75]. Besides, bands at 2927 $cm^{-1}$ (in MD), 2909 $cm^{-1}$ (in GA), 2962, and 2932 $cm^{-1}$ (in SP) of the symmetric and asymmetric C—H stretching [33,76–78] of the $CH_2$ group [79–81], shifted to higher frequencies in the range 2930–2935 $cm^{-1}$. This suggests an interaction between extracted aromatic and wall materials. In the SP, a band was observed at 2874 $cm^{-1}$, which shifted to 2877 $cm^{-1}$ in the sample M2 (containing 30 % SP). A new lower band was observed at 1734 $cm^{-1}$, which decreases its intensity when all three matrices are combined, it could represent the hydroxyl groups (-OH) of MD, GA, and the hydrophilic region (hydroxyl group) of anthocyanins, which can form hydrogen bonds with the amide or carboxyl (-COOH) groups of SP. The new broad band at around 1716 $cm^{-1}$ suggests ester bond C═O stretching vibrations between the phenolic present -OH groups in the extract and carboxylic acid (-COOH) of proteins or carbohydrates in all microcapsule formulations. The bands at 1646–1642 $cm^{-1}$ and 1635–1632 $cm^{-1}$ observed in the formulations are related to amide I, due to the interaction of high concentration of MD and SP with anthocyanin, while the amide II band at 1538–1534 $cm^{-1}$ appeared in the samples (M2, M3, and M10) due to the high concentration of SP and GA [23]. This is in good agreement with other reports indicating that the amide region suggests an interaction between anthocyanin and wall materials, mainly through hydrogen bonding [82] or electrostatic interaction [71]. Furthermore, the complexation of anthocyanin with SP through hydrophobic interaction had little effect on its secondary structure [83]. Also, the broad shoulder bands at 1400–1335 $cm^{-1}$ and the increased intensity of the band around 1219–1200 $cm^{-1}$ after encapsulation are attributed to the C—O angular deformation of the phenol hydroxyl group, or phenolic esters attached to polysaccharides, and it is in concordance with the

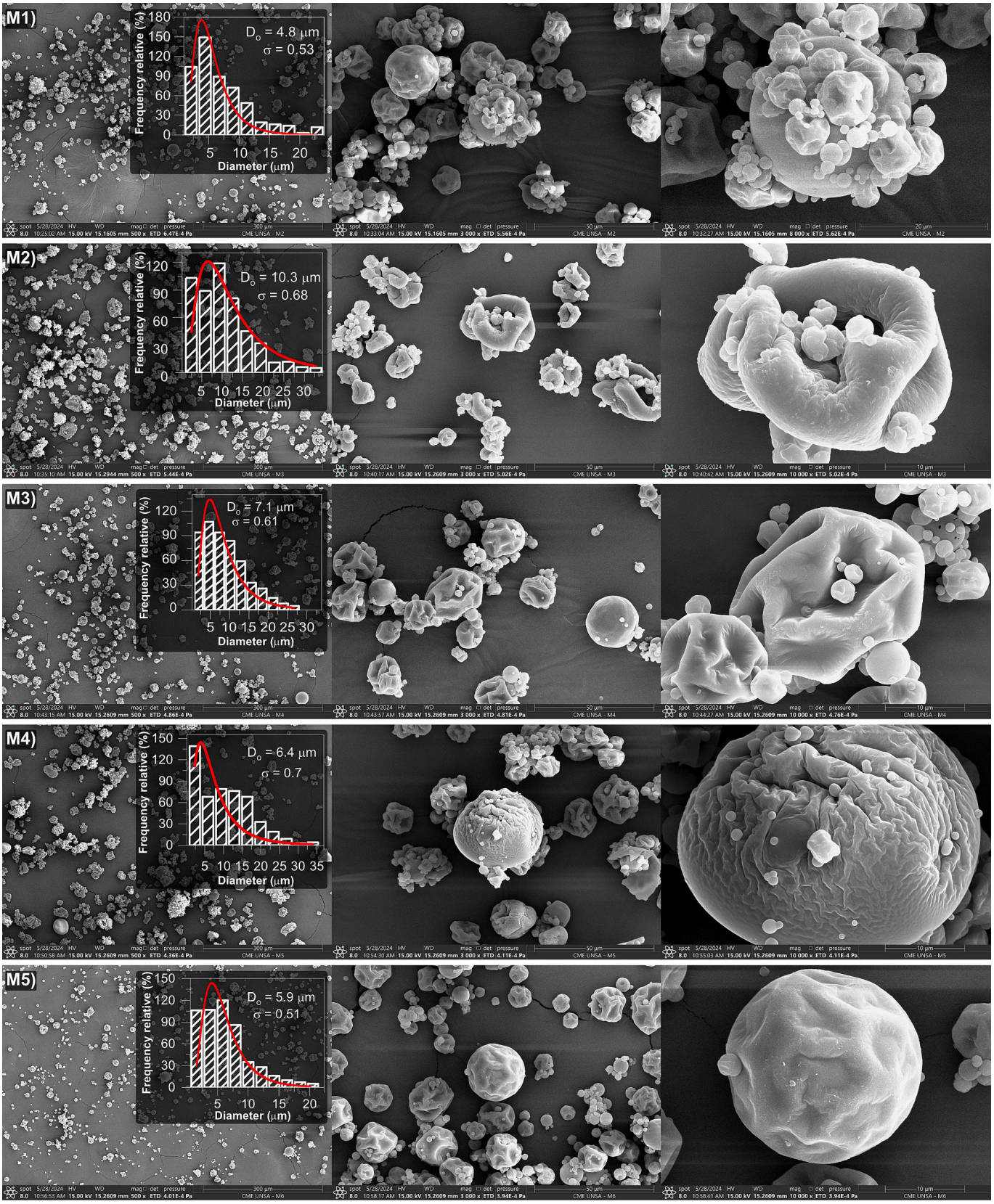



**Fig. 6.** Scanning electron microscopy (SEM) images of MAP formulations (M1-M5) at magnifications of 500×, 3000×, and 10,000×.

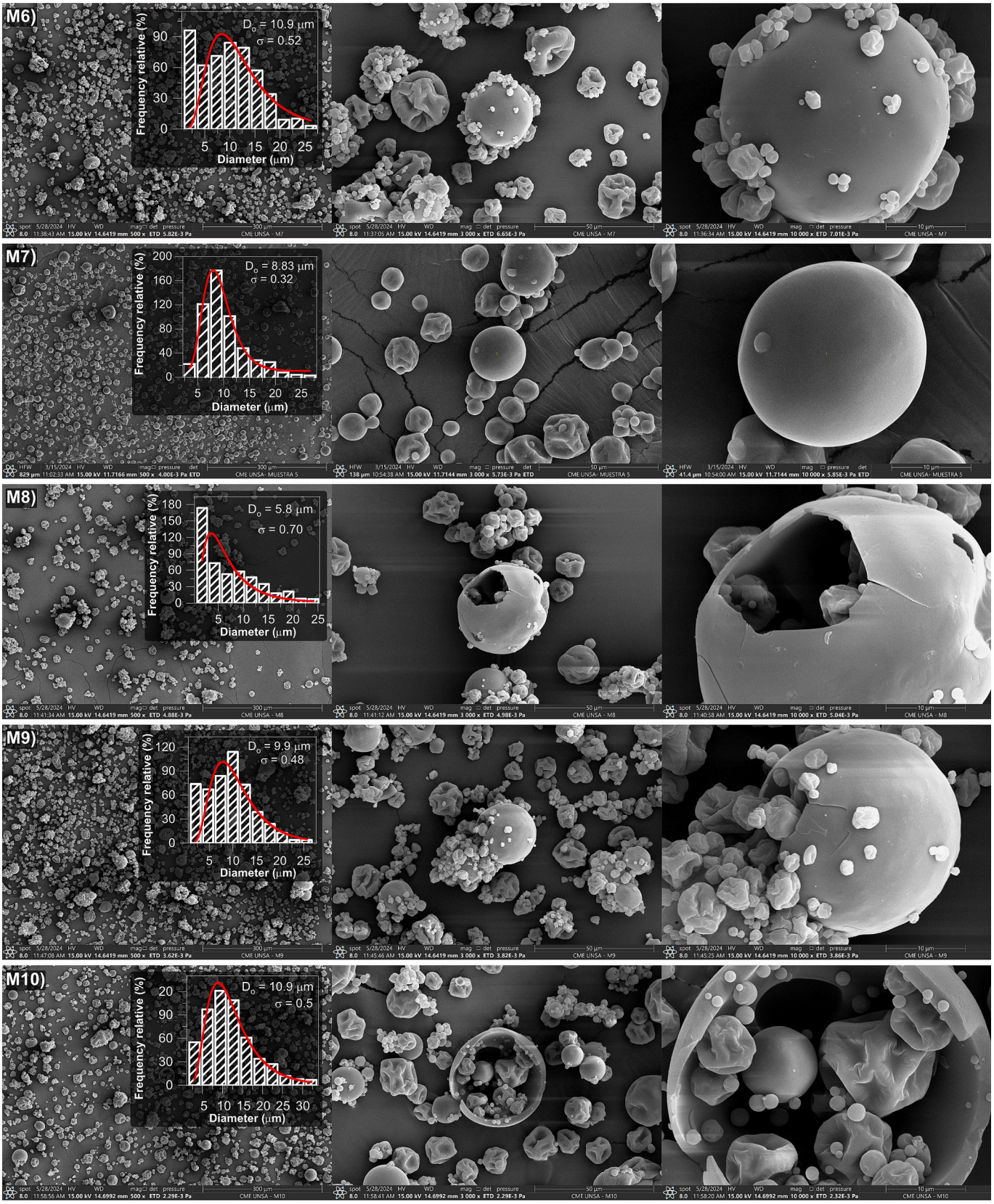



**Fig. 7.** Scanning electron microscopy (SEM) images of MAP formulations (M6-M10) at magnifications of 500×, 3000×, and 10,000×.

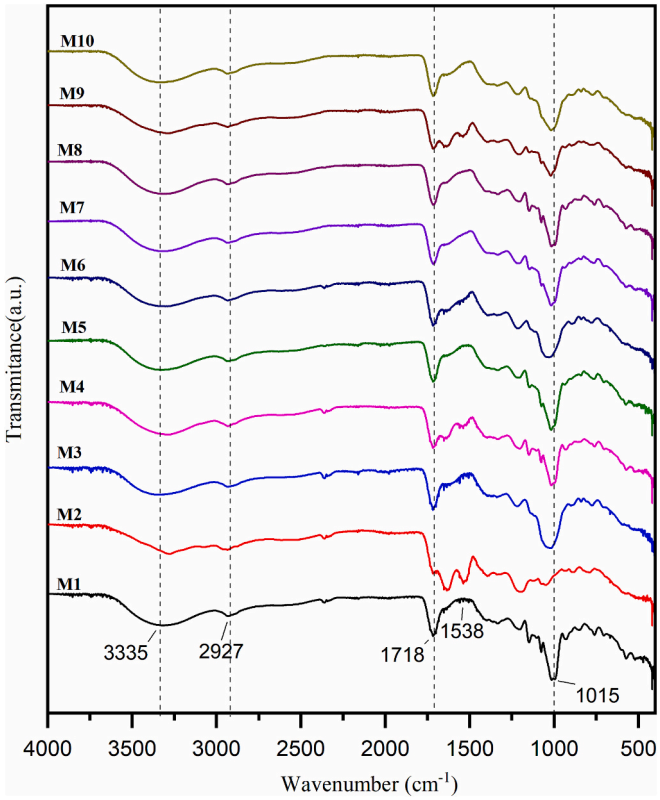



**Fig. 8.** Attenuated total reflectance–Fourier transform infrared spectroscopy (ATR–FTIR) spectra of MAP formulations (M1–M10).

C═O stretching and amide II vibrations mentioned above [84]. A band around 1149–1142 $cm^{-1}$ (in all samples that contain MD), 1076 $cm^{-1}$, 1018–1015 $cm^{-1}$ (in all samples that contain MD), and 1073 $cm^{-1}$ (in samples that containing >30 % SP) are related to C—O stretching vibration bond [82] in the C-O-H of wall materials. A lower shoulder band at 1139 $cm^{-1}$, related to C—O stretching [85], was observed in all samples that contained GA. Furthermore, the microcapsules with concentrations >15 % of MD (M1, M4, M5 and M8) exhibit a small shift in their bands similar to those of MD (from 992 $cm^{-1}$ to 995 $cm^{-1}$, from 930 $cm^{-1}$ to 931–933 $cm^{-1}$, from 850 $cm^{-1}$ to 852 $cm^{-1}$, from 761 $cm^{-1}$ to 762 $cm^{-1}$, 705 $cm^{-1}$ does not change, from 600 $cm^{-1}$ to 602 and 606 $cm^{-1}$, and from 572 $cm^{-1}$ to 573–576 $cm^{-1}$) below the bands at 1149 $cm^{-1}$, which confirms the effectiveness of MD in protecting the antioxidant compounds present in the core of the microcapsules. The microcapsules with concentrations below 10 % of MD and 20 % GA (M7, M9, M10) exhibit similar bands, with few differences, possibly due to the addition of GA. While the microcapsules with a predominance of 30 % GA (M3 and M6) exhibit a slight shift in their bands (909 $cm^{-1}$, from 887 $cm^{-1}$ to 890 $cm^{-1}$, from 838 $cm^{-1}$ to 840 $cm^{-1}$, from 807 $cm^{-1}$ to 804 $cm^{-1}$, and from 771 $cm^{-1}$ to 775 $cm^{-1}$). On the other hand, the SP exhibits only two bands at 981 $cm^{-1}$ related to vibrational modes of the α-(1 ↔ 1)-glycosidic bond or C–O–C vibration [86] or the C—H off-plane coiling vibration band [87], and 740 $cm^{-1}$ and these bands disappear after encapsulation. In all encapsulated samples, the bands at 705 $cm^{-1}$, 668 $cm^{-1}$, and 573–576 $cm^{-1}$ are related to the O—H deformation [21,88] of carbohydrate skeletal vibration [89] and protein [90].

The overall findings confirm that PCCE was successfully encapsulated within the wall materials in all MAP formulations, as evidenced by the weakening of the characteristic anthocyanin bands in the FTIR [58]. This reduction in absorption intensity suggests that non-covalent interactions, such as hydrophobic interactions, van der Waals forces, and hydrogen bonding, occurred between PCCE and the wall materials. These interactions, associated with reduced bonding energies, facilitated the successful encapsulation of PCCE.

Furthermore, the formation of hydrogen bonds between PCCE and the wall materials led to characteristic band shifts, further supporting the efficiency of the encapsulation process and suggesting enhanced stability of the anthocyanins within the microcapsules. Similar spectroscopic analyses in related encapsulation systems have shown that most absorption bands originate from wall material interactions, with partially overlapping yet distinguishable signals from the encapsulated core, indicating the presence of chemical interactions without necessarily altering the crystalline structure [91].

## 4. Conclusion

Natural extracts derived from purple corn cobs are rich in antioxidant compounds that were successfully microencapsulated with wall materials using ten different formulations consisting of maltodextrin, gum arabic, and soy protein isolate. Encapsulation efficiencies for all formulations were nearly 96 %, except for the soy protein isolate formulation, which had an efficiency of 95 %. Microcapsules from formulations M5 and M6 exhibited the highest anthocyanin and total phenolic content. Structural analysis revealed that the different wall materials did not significantly alter the semi-crystalline structure of the encapsulating matrices. Furthermore, using encapsulating agents in equal proportions, as in formulation M7, it was observed that microcapsules with smoother and more rounded surfaces showed fewer irregularities compared to those prepared with maltodextrin, soy protein, or gum arabic alone. Microcapsules showed excellent encapsulation efficiency and stability, particularly in formulations combining wall materials, highlighting the advantage of synergistic interactions over individual agents. The spectral analysis of the microcapsule formulations demonstrated significant interactions between the PCCE and wall materials, evidenced by shifts in vibrational bands, hydrogen bonding, and ester bond formation, which could exhibit hydrophobic characteristics. These interactions, particularly in the amide and carbohydrate regions, confirm the effectiveness of wall materials (SP, MD, GA) in stabilizing and protecting bioactive compounds during encapsulation, thereby enhancing their functional properties and potential applications. The microcapsule formulations examined in this study exhibited significant pH sensitivity, responding distinctly under acidic, neutral, and alkaline conditions (pH 4, 7, and 10). This pH-responsive behavior highlights their versatility and potential applications in intelligent systems, such as pH-sensitive sensors for food packaging. Furthermore, the structural stability of the encapsulated compounds across different pH levels indicates that the wall materials provided effective protection for the active core, enhancing their functionality under varying environmental conditions. Although this study optimized microencapsulation efficiency and confirmed antioxidant properties and pH stability under controlled laboratory conditions, it did not evaluate microcapsule performance in complex food matrices or biological systems. In addition, long-term stability was not assessed. These limitations highlight the need for future research to evaluate microcapsule stability and functionality during extended storage and under food-relevant processing conditions, as well as evaluate bioavailability and antioxidant activity under variable pH conditions. Such research would support the potential application of this technology in the food industry.

## CRediT authorship contribution statement

**Milagros Sofia Bustamante-Bernedo:** Validation, Methodology, Investigation, Formal analysis, Data curation, Conceptualization, Writing – review & editing, Writing – original draft. **Lizbet León Félix:** Validation, Supervision, Resources, Project administration, Methodology, Investigation, Funding acquisition, Conceptualization, Writing – review & editing, Writing – original draft. **Nils Leander Huamán-Castilla:** Methodology, Investigation, Writing – review & editing, Writing – original draft. **Silvia Ponce:** Investigation, Writing – review &

editing. **David G. Pacheco-Salazar:** Supervision, Investigation, Writing – review & editing, Writing – original draft.

## Declaration of competing interest

The authors declare that they have no known competing financial interests or personal relationships that could have appeared to influence the work reported in this paper.

## Acknowledgments

This work was supported by CONCYTEC through the PROCIENCIA program (contract N° PE501077940-2022-PROCIENCIA). Evaluated purple corn samples are from Peru and have been accessed under Contract N° 009-2024-MIDAGRI-INIA/DGIA (Perú) granted by Resolución Directoral N° 014-2024-INIA-DGIA.

## Appendix A. Supplementary data

Supplementary data to this article can be found online at https://doi.org/10.1016/j.ijbiomac.2025.144937.

## References

[1] M.L. Rojas, K. Ramirez, G. Linares, Biocompounds recovery from purple corn cob by-product: extraction kinetics, thermal and physicochemical stability of liquid and powdered anthocyanin-rich extract, Food Bioprod. Process. 149 (2025) 25–35, https://doi.org/10.1016/J.FBP.2024.11.010.

[2] B.F. Feitosa, B.L.A. Decker, E.S. de Brito, S. Rodrigues, L.R.B. Mariutti, Microencapsulation of anthocyanins as natural dye extracted from fruits – a systematic review, Food Chem. 424 (2023), https://doi.org/10.1016/j.foodchem.2023.136361.

[3] G. Rolandelli, L.C. Favre, T.R. Aguirre-Calvo, A.E. Farroni, M. del P. Buera, C. dos Santos Ferreira, An optimized purple corn cob extract as an ingredient for the development of maize-based extrudates with novel characteristics, J. Cereal Sci. 114 (2023) 103809, https://doi.org/10.1016/J.JCS.2023.103809.

[4] H. Yong, J. Liu, Recent advances in the preparation, physical and functional properties, and applications of anthocyanins-based active and intelligent packaging films, Food Packag. Shelf Life 26 (2020), https://doi.org/10.1016/j.fpsl.2020.100550.

[5] L. Wang, F. Peng, S. Yang, Y. Yang, H. Jiang, W. Huang, Y. Bian, B. Li, Antioxidant capacity and in vitro lipid-lowering effect of purple corn (Zea mays L.) processed by different methods, Ind Crops Prod 222 (2024) 120084, https://doi.org/10.1016/J.INDCROP.2024.120084.

[6] Y.M. Monroy, R.A.F. Rodrigues, A. Sartoratto, F.A. Cabral, Extraction of bioactive compounds from cob and pericarp of purple corn (Zea mays L.) by sequential extraction in fixed bed extractor using supercritical CO2, ethanol, and water as solvents, J. Supercrit. Fluids 107 (2016) 250–259, https://doi.org/10.1016/J.SUPFLU.2015.09.020.

[7] S. Pirsa, I.K. Sani, S.S. Mirtalebi, Nano-biocomposite based color sensors: investigation of structure, function, and applications in intelligent food packaging, Food Packag. Shelf Life 31 (2022) 100789, https://doi.org/10.1016/J.FPSL.2021.100789.

[8] L. Fan, Y. Chen, Y. Zeng, Z. Yu, Y. Dong, D. Li, C. Zhang, C. Ye, Application of visual intelligent labels in the assessment of meat freshness, Food Chem. 460 (2024) 140562, https://doi.org/10.1016/J.FOODCHEM.2024.140562.

[9] X. Wu, X. Yan, J. Zhang, X. Wu, Q. Zhang, B. Zhang, Intelligent films based on dual-modified starch and microencapsulated Aronia melanocarpa anthocyanins: functionality, stability and application, Int. J. Biol. Macromol. 275 (2024) 134076, https://doi.org/10.1016/J.IJBIOMAC.2024.134076.

[10] K. Rojas, M.G. Verdugo-Molinares, A.A. Vallejo-Cardona, Use of encapsulating polymers of active compounds in the pharmaceutical and food industry, Food Chemistry Advances 4 (2024) 100619, https://doi.org/10.1016/J.FOCHA.2024.100619.

[11] P. Cazón, A. Sanches Silva, Natural pigments from food wastes: new approaches for the extraction and encapsulation, Curr. Opin. Green Sustain. Chem. 47 (2024) 100929, https://doi.org/10.1016/J.COGSC.2024.100929.

[12] H. Xue, J. Zhao, Y. Wang, Z. Shi, K. Xie, X. Liao, J. Tan, Factors affecting the stability of anthocyanins and strategies for improving their stability: a review, Food Chem X 24 (2024) 101883, https://doi.org/10.1016/J.FOCHX.2024.101883.

[13] L.S. Chua, H.Y. Thong, J. Soo, Effect of pH on the extraction and stability of anthocyanins from jaboticaba berries, Food Chemistry Advances 5 (2024) 100835, https://doi.org/10.1016/J.FOCHA.2024.100835.

[14] O. Jiménez-González, J.Á. Guerrero-Beltrán, Extraction, microencapsulation, color properties, and experimental design of natural pigments obtained by spray drying, Food Eng. Rev. 13 (2021) 769–811, https://doi.org/10.1007/s12393-021-09288-7.

[15] N. Moshfegh, M. Niakousary, S.M.H. Hosseini, S.M. Mazloomi, A. Abbasi, Effect of maltodextrin and Persian gum as wall materials and tannic acid as copigment on some properties of encapsulated sour cherry anthocyanin microcapsules, Food Chem. 463 (2025) 141165, https://doi.org/10.1016/J.FOODCHEM.2024.141165.

[16] S. Jafari, S.M. Jafari, M. Ebrahimi, I. Kijpatanasilp, K. Assatarakul, A decade overview and prospect of spray drying encapsulation of bioactives from fruit products: characterization, food application and in vitro gastrointestinal digestion, Food Hydrocoll. 134 (2023) 108068, https://doi.org/10.1016/J.FOODHYD.2022.108068.

[17] S.P. Tan, T.C. Kha, S.E. Parks, C.E. Stathopoulos, P.D. Roach, Effects of the spray-drying temperatures on the physiochemical properties of an encapsulated bitter melon aqueous extract powder, Powder Technol. 281 (2015) 65–75, https://doi.org/10.1016/J.POWTEC.2015.04.074.

[18] R. Tang, Y. He, K. Fan, Recent advances in stability improvement of anthocyanins by efficient methods and its application in food intelligent packaging: a review, Food Biosci. 56 (2023) 103164, https://doi.org/10.1016/J.FBIO.2023.103164.

[19] B.L.A. Decker, E. de C. Miguel, T.V. Fonteles, F.A.N. Fernandes, S. Rodrigues, Impact of spray drying on the properties of grape pomace extract powder, Processes 12 (7) (2024) 1390, https://doi.org/10.3390/pr12071390.

[20] Y. Deng, G. Liu, H. Zhang, P. Zhou, X. Tang, P. Li, Z. Zhao, Y. Zhang, Z. Wang, Z. Wei, M. Zhang, Effects of wall materials on the physicochemical properties of spray-dried bitter gourd (Momordica charantia L.) powders, NPJ Sci Food 8 (2024) 37, https://doi.org/10.1038/s41538-024-00278-7.

[21] E.J.G. Laureanti, T.S. Paiva, L.M. de Matos Jorge, R.M.M. Jorge, Microencapsulation of bioactive compound extracts using maltodextrin and gum arabic by spray and freeze-drying techniques, Int. J. Biol. Macromol. 253 (2023) 126969, https://doi.org/10.1016/j.ijbiomac.2023.126969.

[22] C.T. Nguyen, K. Nguyen Di, H.C. Phan, T.C. Kha, H.C. Nguyen, Microencapsulation of noni fruit extract using gum arabic and maltodextrin – optimization, stability and efficiency, Int. J. Biol. Macromol. 269 (2024) 132217, https://doi.org/10.1016/j.ijbiomac.2024.132217.

[23] E. Karrar, A.A. Mahdi, S. Sheth, I.A. Mohamed Ahmed, M.F. Manzoor, W. Wei, X. Wang, Effect of maltodextrin combination with gum arabic and whey protein isolate on the microencapsulation of gurum seed oil using a spray-drying method, Int. J. Biol. Macromol. 171 (2021) 208–216, https://doi.org/10.1016/j.ijbiomac.2020.12.045.

[24] Z. Akbarbaglu, S.H. Peighambardoust, K. Sarabandi, S.M. Jafari, Spray drying encapsulation of bioactive compounds within protein-based carriers; different options and applications, Food Chem. 359 (2021) 129965, https://doi.org/10.1016/J.FOODCHEM.2021.129965.

[25] I. Khalifa, M. Li, T. Mamet, C. Li, Maltodextrin or gum Arabic with whey proteins as wall-material blends increased the stability and physiochemical characteristics of mulberry microparticles, Food Biosci. 31 (2019) 100445, https://doi.org/10.1016/J.FBIO.2019.100445.

[26] E.C.Q. Lacerda, V.M.D.A. Calado, M. Monteiro, P.V. Finotelli, A.G. Torres, D. Perrone, Starch, inulin and maltodextrin as encapsulating agents affect the quality and stability of jussara pulp microparticles, Carbohydr. Polym. 151 (2016) 500–510, https://doi.org/10.1016/J.CARBPOL.2016.05.093.

[27] M.S. Bustamante-Bernedo, L.L. Félix, E. Gutiérrez-Pineda, N.L. Huamán-Castilla, J. L. Solis, M.M.G. León, I.R. Montoya-Matos, J.C. Yacono-Llanos, D.G. Pacheco-Salazar, Development of antioxidant films based on anthocyanin microcapsules extracted from purple corn cob and incorporated into a chitosan matrix, Int. J. Biol. Macromol. 284 (2025) 137658, https://doi.org/10.1016/J.IJBIOMAC.2024.137658.

[28] R. Zhang, L. Zhou, J. Li, H. Oliveira, N. Yang, W. Jin, Z. Zhu, S. Li, J. He, Microencapsulation of anthocyanins extracted from grape skin by emulsification/internal gelation followed by spray/freeze-drying techniques: characterization, stability and bioaccessibility, LWT 123 (2020) 109097, https://doi.org/10.1016/J.LWT.2020.109097.

[29] M.M. Giusti, R.E. Wrolstad, Characterization and measurement of anthocyanins by UV-visible spectroscopy, Curr. Protocol Food Anal. Chem. 00 (2001), https://doi.org/10.1002/0471142913.faf0102s00.

[30] S.M. Parí, M.L.M. Juárez, F.Z. Vilca, O.M.L. Vilca, E.E.A. Alca, E. Escobedo-Pacheco, N.L. Huamán-Castilla, Alternative green extraction techniques to enhance recovery of antioxidant compounds from red peel prickly pear (*Opuntia ficus-indica* L. Miller), Discover Food 4 (2024) 58, https://doi.org/10.1007/s44187-024-00140-5.

[31] S. Rosales-Chimal, R.O. Navarro-Cortez, L.A. Bello-Perez, A. Vargas-Torres, H. M. Palma-Rodríguez, Optimal conditions for anthocyanin extract microencapsulation in taro starch: physicochemical characterization and bioaccessibility in gastrointestinal conditions, Int. J. Biol. Macromol. 227 (2023) 83–92, https://doi.org/10.1016/J.IJBIOMAC.2022.12.136.

[32] J.N. de Carvalho Alves, N.L. Oliveira, A.C.F. de Oliveira Meira, L.A.S. Pio, J.V. de Resende, Valorization of the peel of pitaya's fruit (*Hylocereus polyrhizus*) producing betalain-rich freeze-dried microparticles, Waste Biomass Valor. 15 (2024) 1097–1111, https://doi.org/10.1007/s12649-023-02234-0.

[33] L. Tang, H. Liu, G. Huang, Z. Yuan, M. Fu, Z. Bu, J. Wen, Y. Xu, The structural characterization, physicochemical properties, and stability of gardenia yellow pigment microcapsules, LWT 162 (2022) 113507, https://doi.org/10.1016/j.lwt.2022.113507.

[34] J. Grgić, G. Šelo, M. Planinić, M. Tišma, A. Bucić-Kojić, Role of the encapsulation in bioavailability of phenolic compounds, Antioxidants 9 (2020) 923, https://doi.org/10.3390/antiox9100923.

[35] S. Akhavan Mahdavi, S.M. Jafari, E. Assadpoor, D. Dehnad, Microencapsulation optimization of natural anthocyanins with maltodextrin, gum Arabic and gelatin, Int. J. Biol. Macromol. 85 (2016) 379–385, https://doi.org/10.1016/j.ijbiomac.2016.01.011.

[36] O. Norkaew, P. Thitisut, S. Mahatheeranont, B. Pawin, P. Sookwong, S. Yodpitak, A. Lungkaphin, Effect of wall materials on some physicochemical properties and release characteristics of encapsulated black rice anthocyanin microcapsules, Food Chem. 294 (2019) 493–502, https://doi.org/10.1016/j.foodchem.2019.05.086.
[37] M. Igual, S. Ramires, L.H. Mosquera, N. Martínez-Navarrete, Optimization of spray drying conditions for lulo (Solanum quitoense L.) pulp, Powder Technol. 256 (2014) 233–238, https://doi.org/10.1016/J.POWTEC.2014.02.003.
[38] A. Al-Hamayda, B. Abu-Jdayil, M. Ayash, J. Tannous, Advances in microencapsulation techniques using Arabic gum: a comprehensive review, Ind Crops Prod 205 (2023) 117556, https://doi.org/10.1016/J.INDCROP.2023.117556.
[39] W. Deng, X. Li, G. Ren, Q. Bu, Y. Ruan, Y. Feng, B. Li, Stability of purple corn anthocyanin encapsulated by maltodextrin, and its combinations with gum arabic and whey protein isolate, Foods 12 (2023) 2393, https://doi.org/10.3390/foods12122393.
[40] A. Ali, C. Wan, M. Lin, S. Flint-Garcia, B. Vardhanabhuti, P. Somavat, Microencapsulation of highly concentrated polyphenolic compounds from purple corn pericarp by spray-drying with various biomacromolecules, Int. J. Biol. Macromol. 272 (2024) 132938, https://doi.org/10.1016/j.ijbiomac.2024.132938.
[41] S. Mohammadalinejhad, A. Almonaitytė, I.-J. Jensen, M. Kurek, J. Lerfall, Alginate microbeads incorporated with anthocyanins from purple corn (e c mays L.) using electrostatic extrusion: microencapsulation optimization, characterization, and stability studies, Int. J. Biol. Macromol. 246 (2023) 125684, https://doi.org/10.1016/j.ijbiomac.2023.125684.
[42] L. Stoll, T.M.H. Costa, A. Jablonski, S.H. Flôres, A. de Oliveira Rios, Microencapsulation of anthocyanins with different wall materials and its application in active biodegradable films, Food Bioproc. Tech. 9 (2016) 172–181, https://doi.org/10.1007/s11947-015-1610-0.
[43] J. de C.G. Rocha, F.A.R. de Barros, Í.T. Perrone, K.W.C. Viana, G.M. Tavares, R. Stephani, P.C. Stringheta, Microencapsulation by atomization of the mixture of phenolic extracts, Powder Technol. 343 (2019) 317–325, https://doi.org/10.1016/j.powtec.2018.11.040.
[44] N. Sendri, S. Singh, V. Bhatt, P. Bhatt, P. Bhandari, Valorization of red cabbage pomace for stabilization of anthocyanins in Rhododendron arboreum, Ind. Crop. Prod. 187 (2022) 115371, https://doi.org/10.1016/j.indcrop.2022.115371.
[45] T.O. Hay, M.A. Fitzgerald, J.R. Nastasi, Systematic application of UPLC-Q-ToF-MS/MS coupled with chemometrics for the identification of natural food pigments from Davidson plum and native currant, Food Chem X 25 (2025) 102072, https://doi.org/10.1016/J.FOCHX.2024.102072.
[46] F. Xu, Y. Yan, X. Huang, D. Yun, C. Tang, J. Liu, Modulating the functionality of black wolfberry anthocyanins-based freshness indicators by adjusting the pH value of film-forming solution, Food Biosci. 53 (2023) 102764, https://doi.org/10.1016/J.FBIO.2023.102764.
[47] D.F. Rocha-Parra, M.C. Lanari, M.C. Zamora, J. Chirife, Influence of storage conditions on phenolic compounds stability, antioxidant capacity and colour of freeze-dried encapsulated red wine, LWT 70 (2016) 162–170, https://doi.org/10.1016/J.LWT.2016.02.038.
[48] P. Moser, V.R.N. Telis, N. de Andrade Neves, E. García-Romero, S. Gómez-Alonso, I. Hermosín-Gutiérrez, Storage stability of phenolic compounds in powdered BRS Violeta grape juice microencapsulated with protein and maltodextrin blends, Food Chem. 214 (2017) 308–318, https://doi.org/10.1016/J.FOODCHEM.2016.07.081.
[49] M. Ahmad, B. Ashraf, A. Gani, A. Gani, Microencapsulation of saffron anthocyanins using β glucan and β cyclodextrin: microcapsule characterization, release behaviour & antioxidant potential during in-vitro digestion, Int. J. Biol. Macromol. 109 (2018) 435–442, https://doi.org/10.1016/J.IJBIOMAC.2017.11.122.
[50] Y. Lei, Q. Yao, Z. Jin, Y.C. Wang, Intelligent films based on pectin, sodium alginate, cellulose nanocrystals, and anthocyanins for monitoring food freshness, Food Chem. 404 (2023) 134528, https://doi.org/10.1016/J.FOODCHEM.2022.134528.
[51] R.V. Wagh, A. Khan, R. Priyadarshi, P. Ezati, J.W. Rhim, Cellulose nanofiber-based multifunctional films integrated with carbon dots and anthocyanins from Brassica oleracea for active and intelligent food packaging applications, Int. J. Biol. Macromol. 233 (2023) 123567, https://doi.org/10.1016/J.IJBIOMAC.2023.123567.
[52] Y. Zhao, L. Gao, J. Wang, Z. Xue, M. Zhang, X. Ma, G. Wang, S. Lv, Preparation and application of pH-sensitive film containing anthocyanins extracted from Lycium ruthenicum Murr, Materials 16 (2023) 3828, https://doi.org/10.3390/ma16103828.
[53] B. Merz, C. Capello, G.C. Leandro, D.E. Moritz, A.R. Monteiro, G.A. Valencia, A novel colorimetric indicator film based on chitosan, polyvinyl alcohol and anthocyanins from jambolan (Syzygium cumini) fruit for monitoring shrimp freshness, Int. J. Biol. Macromol. 153 (2020) 625–632, https://doi.org/10.1016/j.ijbiomac.2020.03.048.
[54] Y. Cao, Q. Gou, Z. Song, L. Zhang, Q. Yu, X. Zhu, S. Li, Smart carrageenan/carboxymethyl cellulose films combined with zein/gellan gum microcapsules encapsulated by composite anthocyanins for chilled beef freshness monitoring, Food Hydrocoll. 153 (2024) 110059, https://doi.org/10.1016/J.FOODHYD.2024.110059.
[55] B.E. Teixeira-Costa, W.H. Ferreira, F.M. Goycoolea, B.S. Murray, C.T. Andrade, Improved antioxidant and mechanical properties of food packaging films based on chitosan/deep eutectic solvent, containing açaí-filled microcapsules, Molecules 28 (2023) 1507, https://doi.org/10.3390/molecules28031507.
[56] J. Dai, Y. Ruan, Y. Feng, B. Li, Physical properties, α-glucosidase inhibitory activity, and digestive stability of four purple corn cob anthocyanin complexes, Foods 11 (2022) 3665, https://doi.org/10.3390/foods11223665.
[57] A.P. da Fonseca Machado, C. Alves Rezende, R. Alexandre Rodrigues, G. Fernández Barbero, P. de Tarso Vieira e Rosa, J. Martínez, Encapsulation of anthocyanin-rich extract from blackberry residues by spray-drying, freeze-drying and supercritical antisolvent, Powder Technol. 340 (2018) 553–562, https://doi.org/10.1016/J.POWTEC.2018.09.063.
[58] Y. Shi, X. Chen, Q. Gao, Y. Zou, D. Xing, R. Chen, X. He, Q. Li, Preparation and chemical properties of microencapsulation developed with mulberry anthocyanins and silk fibroin, Ind Crops Prod 212 (2024) 118383, https://doi.org/10.1016/j.indcrop.2024.118383.
[59] S. Thaher, S. Anggrahini, C. Hidayat, H. Hariadi, Microencapsulation of orange-fleshed sweet potato (*Ipomoea batatas*) carotenoid extract by spray-drying with maltodextrin and whey protein concentrates, Advances in Food Science, Sustainable Agriculture and Agroindustrial Engineering 5 (2022) 130–137, https://doi.org/10.21776/ub.afssaae.2022.005.02.2.
[60] Y.-R. Kang, Y.-K. Lee, Y.J. Kim, Y.H. Chang, Characterization and storage stability of chlorophylls microencapsulated in different combination of gum Arabic and maltodextrin, Food Chem. 272 (2019) 337–346, https://doi.org/10.1016/j.foodchem.2018.08.063.
[61] G.R. Marques, R.V. de B. Fernandes, S.V. Borges, D.A. Botrel, Influence of spray-drying conditions on physical and morphological characteristics of microencapsulated benzoic acid, Food Bioprocess Technol. 9 (2016) 1969–1978, https://doi.org/10.1007/s11947-016-1784-0.
[62] M.T.L. Pereira, M.P. Cavalcante, S.F. da Silva, Y. Sensheng, S. dos S. Silva, A.C. de Aquino, Í.M. da S. Araújo, E.S. Dantas, B.M.B. da Silva, E. de G. Alves Filho, L.M. A. e Silva, S.V. Frota Gaban, Effect of different carrier agents on the yield of powered plant beverage obtained by spray drying and characterization of physicochemical properties, ACS Food Sci. Technol. 4 (2024) 2392–2399, https://doi.org/10.1021/acsfoodscitech.4c00478.
[63] A.A. Mahdi, J.K. Mohammed, W. Al-Ansi, A.D.S. Ghaleb, Q.A. Al-Maqtari, M. Ma, M.I. Ahmed, H. Wang, Microencapsulation of fingered citron extract with gum arabic, modified starch, whey protein, and maltodextrin using spray drying, Int. J. Biol. Macromol. 152 (2020) 1125–1134, https://doi.org/10.1016/j.ijbiomac.2019.10.201.
[64] A.S. Alameen, S.B. Undre, P.B. Undre, Functionalization of ZnO nanoparticles and their antimicrobial activity: in vitro, Nano-Structures & Nano-Objects 39 (2024) 101314, https://doi.org/10.1016/J.NANOSO.2024.101314.
[65] S. Rojas-Moreno, F. Cárdenas-Bailón, G. Osorio-Revilla, T. Gallardo-Velázquez, J. Proal-Nájera, Effects of complex coacervation-spray drying and conventional spray drying on the quality of microencapsulated orange essential oil, J. Food Meas. Charact. 12 (2018) 650–660, https://doi.org/10.1007/s11694-017-9678-z.
[66] J. Righi da Rosa, G.L. Nunes, M.H. Motta, J.P. Fortes, G.C. Cezimbra Weis, L. H. Rychecki Heckttheuer, E.I. Muller, C. Ragagnin de Menezes, C. Severo da Rosa, Microencapsulation of anthocyanin compounds extracted from blueberry (Vaccinium spp.) by spray drying: characterization, stability and simulated gastrointestinal conditions, Food Hydrocoll. 89 (2019) 742–748, https://doi.org/10.1016/j.foodhyd.2018.11.042.
[67] G. Nelson, Microencapsulated colourants for technical textile application, in: Advances in the Dyeing and Finishing of Technical Textiles, Elsevier, 2013, pp. 78–104, https://doi.org/10.1533/9780857097613.1.78.
[68] J.K.S. Andrade, M. Denadai, G.R.S. Andrade, C. da Cunha Nascimento, P. F. Barbosa, M.S. Jesus, N. Narain, Development and characterization of microencapsules containing spray dried powder obtained from Brazilian brown, green and red propolis, Food Res. Int. 109 (2018) 278–287, https://doi.org/10.1016/J.FOODRES.2018.04.048.
[69] Z.-H. Zhang, X. Li, A. Ma, X. Gao, S. Zhu, B. Li, Characteristics of pomegranate (Punica granatum L.) peel polyphenols encapsulated with whey protein isolate and β-cyclodextrin by spray-drying, Int. J. Biol. Macromol. 278 (2024) 135279, https://doi.org/10.1016/j.ijbiomac.2024.135279.
[70] S. Thummajitsakul, P. Paensanit, T. Saeieo, J. Sirirat, K. Silprasit, FTIR and multivariate analysis of total phenolic content, antioxidant and anti-amylase activities of extracts and milk of Glycine max L. and Phaseolus vulgaris L, Electron. J. Biotechnol. 64 (2023) 69–75, https://doi.org/10.1016/j.ejbt.2023.04.001.
[71] Y. Tao, P. Wang, J. Wang, Y. Wu, Y. Han, J. Zhou, Combining various wall materials for encapsulation of blueberry anthocyanin extracts: optimization by artificial neural network and genetic algorithm and a comprehensive analysis of anthocyanin powder properties, Powder Technol. 311 (2017) 77–87, https://doi.org/10.1016/J.POWTEC.2017.01.078.
[72] L. Favaro, V. Balcão, L. Rocha, E. Silva, J. Oliveira Jr., M. Vila, M. Tubino, Physicochemical characterization of a crude anthocyanin extract from the fruits of jussara (Euterpe edulis Martius): potential for food and pharmaceutical applications, J. Braz. Chem. Soc. (2018), https://doi.org/10.21577/0103-5053.20180082.
[73] F. Zeng, Y. Ye, J. Liu, P. Fei, Intelligent pH indicator composite film based on pectin/chitosan incorporated with black rice anthocyanins for meat freshness monitoring, Food Chem X 17 (2023), https://doi.org/10.1016/j.fochx.2022.100531.
[74] M. Zhao, W. Cao, L. Li, A. Ren, Y. Ang, J. Chen, B. Bhandari, Z. Wang, X. Ren, G. Ren, X. Duan, Effects of different proteins and maltodextrin combinations as wall material on the characteristics of Cornus officinalis flavonoids microcapsules, Front. Nutr. 9 (2022), https://doi.org/10.3389/fnut.2022.1007863.
[75] K. Sakulnarmrat, I. Konczak, Encapsulation of Melodorum fruticosum Lour. anthocyanin-rich extract and its incorporation into model food, LWT 153 (2022), https://doi.org/10.1016/j.lwt.2021.112546.
[76] A. Todorović, L. Šturm, A. Salević-Jelić, S. Lević, I.G. Osojnik Črnivec, I. Prislan, M. Skrt, A. Bjeković, N. Poklar Ulrih, V. Nedović, Encapsulation of bilberry extract with maltodextrin and gum arabic by freeze-drying: formulation, characterisation, and storage stability, Processes 10 (2022) 1991, https://doi.org/10.3390/pr10101991.

[77] G. Palumbo, M. Górny, J. Banaś, Corrosion inhibition of pipeline carbon steel (N80) in CO2-saturated chloride (0.5 M of KCl) solution using gum arabic as a possible environmentally friendly corrosion inhibitor for shale gas industry, J. Mater. Eng. Perform. 28 (2019) 6458–6470, https://doi.org/10.1007/s11665-019-04379-3.
[78] L. Mary Jayan, K. Venkatesh, I. Jenova, S. Madeswaran, S. Karthikeyan, Preparation and characterization of Li doped-Arabic Gum-PVA polymer electrolyte, Mater Today Proc (2023), https://doi.org/10.1016/j.matpr.2023.02.223.
[79] M. Bashir, S. Haripriya, Assessment of physical and structural characteristics of almond gum, Int. J. Biol. Macromol. 93 (2016) 476–482, https://doi.org/10.1016/j.ijbiomac.2016.09.009.
[80] X. Chen, Y. Ru, F. Chen, X. Wang, X. Zhao, Q. Ao, FTIR spectroscopic characterization of soy proteins obtained through AOT reverse micelles, Food Hydrocoll. 31 (2013) 435–437, https://doi.org/10.1016/j.foodhyd.2012.11.017.
[81] X. Liu, R. Song, W. Zhang, C. Qi, S. Zhang, J. Li, Development of eco-friendly soy protein isolate films with high mechanical properties through HNTs, PVA, and PTGE synergism effect, Sci. Rep. 7 (2017) 44289, https://doi.org/10.1038/srep44289.
[82] M. Mansour, M. Salah, X. Xu, Effect of microencapsulation using soy protein isolate and gum arabic as wall material on red raspberry anthocyanin stability, characterization, and simulated gastrointestinal conditions, Ultrason. Sonochem. 63 (2020) 104927, https://doi.org/10.1016/j.ultsonch.2019.104927.
[83] Y. Wu, Z. Yin, X. Qie, Y. Chen, M. Zeng, Z. Wang, F. Qin, J. Chen, Z. He, Interaction of soy protein isolate hydrolysates with cyanidin-3-O-glucoside and its effect on the in vitro antioxidant capacity of the complexes under neutral condition, Molecules 26 (2021) 1721, https://doi.org/10.3390/molecules26061721.
[84] G. Sassi, S. Shankar, L. Jaiswal, S. Salmieri, S. Karboune, M. Lacroix, Nanoemulsion-based spray-dried formulation of essential oils, whey protein isolate, and maltodextrin: an approach for antifungal preservation of grated mozzarella cheese, Int. Dairy J. 154 (2024) 105919, https://doi.org/10.1016/j.idairyj.2024.105919.
[85] S.A. Al Kiey, M.S. Hasanin, F.E.-T. Heakal, Green and sustainable chitosan–gum Arabic nanocomposites as efficient anticorrosive coatings for mild steel in saline media, Sci. Rep. 12 (2022) 13209, https://doi.org/10.1038/s41598-022-17386-7.
[86] K. Petsong, S. Benjakul, K. Vongkamjan, Optimization of wall material for phage encapsulation via freeze-drying and antimicrobial efficacy of microencapsulated phage against Salmonella, J. Food Sci. Technol. 58 (2021) 1937–1946, https://doi.org/10.1007/s13197-020-04705-x.
[87] N. Liu, P. Qu, H. Huang, Z. Wei, Soybean protein hydrolysate-formaldehyde-urea block copolymer for controlled release fertilizer, Environmental Pollutants and Bioavailability 31 (2019) 94–102, https://doi.org/10.1080/26395940.2019.1589389.
[88] M. Karaaslan, F. Şengün, Ü. Cansu, B. Başyiğit, H. Sağlam, A. Karaaslan, Gum arabic/maltodextrin microencapsulation confers peroxidation stability and antimicrobial ability to pepper seed oil, Food Chem. 337 (2021) 127748, https://doi.org/10.1016/j.foodchem.2020.127748.
[89] T. Hong, J.-Y. Yin, S.-P. Nie, M.-Y. Xie, Applications of infrared spectroscopy in polysaccharide structural analysis: progress, challenge and perspective, Food Chem X 12 (2021) 100168, https://doi.org/10.1016/j.fochx.2021.100168.
[90] S. Mehra, S. Nisar, S. Chauhan, V. Singh, S. Rattan, Soy protein-based hydrogel under microwave-induced grafting of acrylic acid and 4-(4-hydroxyphenyl) butanoic acid: a potential vehicle for controlled drug delivery in oral cavity bacterial infections, ACS Omega 5 (2020) 21610–21622, https://doi.org/10.1021/acsomega.0c02287.
[91] V. Miranda-Linares, D. Quintanar-Guerrero, A. Del Real, M.L. Zambrano-Zaragoza, Spray-drying method for the encapsulation of a functionalized ingredient in alginate-pectin nano- and microparticles loaded with distinct natural actives: stability and antioxidant effect, Food Hydrocoll. 101 (2020) 105560, https://doi.org/10.1016/J.FOODHYD.2019.105560.